UC Irvine
UC Irvine Previously Published Works

Title

Dynamic Low-Level Context for the Detection of Mild Traumatic Brain Injury

Permalink

https://escholarship.org/uc/item/3pq1005g

Journal

IEEE Transactions on Biomedical Engineering, 62(1)

ISSN

Authors

Bianchi, Anthony
Bhanu, Bir
Obenaus, Andre

Publication Date

2015

DOI

Dynamic Low-Level Context for the Detection of Mild Traumatic Brain Injury

Anthony Bianchi*, Bir Bhanu, *Fellow, IEEE*, and Andre Obenaus

Abstract—**Mild traumatic brain injury (mTBI) appears as low contrast lesions in magnetic resonance (MR) imaging. Standard automated detection approaches cannot detect the subtle changes caused by the lesions. The use of context has become integral for the detection of low contrast objects in images. Context is any information that can be used for object detection but is not directly due to the physical appearance of an object in an image. In this paper, new low-level static and dynamic context features are proposed and integrated into a discriminative voxel-level classifier to improve the detection of mTBI lesions. Visual features, including multiple texture measures, are used to give an initial estimate of a lesion. From the initial estimate novel proximity and directional distance, contextual features are calculated and used as features for another classifier. This feature takes advantage of spatial information given by the initial lesion estimate using only the visual features. Dynamic context is captured by the proposed posterior marginal edge distance context feature, which measures the distance from a hard estimate of the lesion at a previous time point. The approach is validated on a temporal mTBI rat model dataset and shown to have improved dice score and convergence compared to other state-of-the-art approaches. Analysis of feature importance and versatility of the approach on other datasets are also provided.**

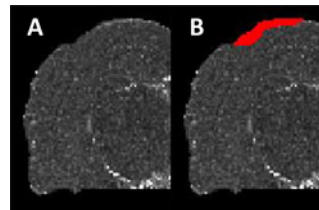*Index Terms*—**Dynamic context, low contrast, magnetic resonance imaging (MRI), traumatic brain injury.**

Fig. 1. T2 weighted MR image of half a coronal slice from the rat model dataset. (a) Original T2 weighted image. (b) Manual detection of the mTBI lesion (highlighted in red). This illustrates the low contrast appearance of mTBI lesions. The manual lesions have been verified by histology in [13].

I. INTRODUCTION

AWARENESS of mild traumatic brain injury (mTBI) has increased dramatically in recent years. Causes of mTBI include sports injuries, automobile accidents, blast injuries in the military, and falls in the workplace [1]. The long-term effects of mTBI are just being recognized, leading to the need for quantitative techniques to characterize and measure the injured tissue.

Clinical evaluation of mTBI has been too qualitative by relying on the Glasgow Coma Scale, to assess loss of consciousness, loss of memory, alteration in mental status, and focal neurological deficits. When imaging is used to assist in diagnosis, MR imaging or computed tomography (CT), a quantitative

measurement of the size and location of injury is typically obtained. The primary focus of imaging is only to assess the presence of a hematoma [1]. Various clinical studies have used manual quantitative analysis to evaluate TBI in MRI [2]–[4]. These studies identified the size and location of the lesions and linked them to long-term neurological effects. Manual analysis has some major downfalls, hours per scan of ROI extraction, a trained operator is required and difficulty in interpreting multiple modalities. Inter- and intraoperator errors can become significant in low contrast images. Interoperator error has been shown to be significant even in higher contrast tumors [5]. However, manual segmentation is considered the "gold standard" and is used as the groundtruth.

Some computational approaches have been proposed for quantifying lesions in moderate to severe TBI [6], which on MRI have high contrast, but these have been unsuccessful when attempting to evaluate the subtle MR signature of mTBI. Lesions caused by mTBI appear as small low contrast regions (see Fig. 1) in both T2 weighted images and T2 maps. The T2 values within these lesions often fall within the range of normal tissue values. Therefore, the T2 value of a voxel cannot be used by itself. In [7], it was shown that there are significant texture changes in brain tissues as a result of mTBI, which provides a measure of the underlying structure of the tissue. Therefore, our proposed approach uses multiple texture measures to improve the discriminative ability of mTBI detection from MR images.

There has been research into advanced MR techniques for detecting mTBI, mainly susceptibility-weighted imaging (SWI) [8]–[10] and diffusion tensor imaging (DTI) [10]–[12]. SWI utilizes the phase image to estimate the magnetic susceptibility in tissue. It has been shown to be more sensitive to blood than CT. However, SWI tends to overestimate a lesion and can give too sharp a contrast leading to hard determination of low-contrast brain structures [9]. DTI measures the "flow" of water in the brain, and has been used to estimate white matter (WM) tracts. Significant changes in WM tracts have been found in patients

with mTBI, but it requires multiple imaging time points or a baseline image [14]. It becomes difficult to evaluate it due to interpatient variations in tractography. This rules out DTI for voxel-based classification. We utilize T2 weighted imaging, a traditional imaging technique as described above.

A measure of contrast within the lesion can be obtained by calculating the contrast-to-noise ratio (CNR). The manually segmented regions are used to calculate the CNR, and a CNR of six on average is obtained. Rajan *et al.* [15] made noise measurements from MRI to estimate the noise variance.

To estimate the mTBI lesion, we use a discriminative approach comprised of voxel level classification utilizing visual and contextual features. Both static and dynamic contextual features are proposed. Static contextual features, proximity and directional, are calculated from local neighborhood information of the posterior marginal probability estimated by a preceding classifier. The dynamic context (posterior marginal edge distance) is calculated from the maximum posterior marginal probability of the cascade of classifiers at a previous time point and then used to estimate the current lesion. Adding these contextual features overcomes the low contrast nature of the lesions.

The paper is organized as follows. Section II presents the related work and the contributions. Section III discusses the technical approach. Section IV describes the experiments and finally Section V provides the conclusion.

II. RELATED WORK AND CONTRIBUTIONS

A. Related Work

Context has been an active area of research in computer vision and can be used to overcome low-contrast detection problems. Context is defined [16] as, "any information that might be relevant to object detection, categorization, and classification tasks, but not directly due to the physical appearance of the object, as perceived by the image acquisition system." Context types that have been described include: local pixels, 2-D scene gist, 3-D geometric, semantic, photogrammetric, illumination, weather, geographic, temporal, and cultural [17]. Context can be split into two types local and global: 1) Local context includes spatial relationships learned at the pixel/region level. It is used in conditional random fields (CRFs) [18] and autocontext [19]. 2) Global context can be thought of as an estimation of the spatial location of an object. In this paper, we exploit low (voxel) level context. Our previous approach [20] uses a contextually driven generative model to estimate the lesion location.

As a starting point, algorithms for multiple Sclerosis (MS) are examined due to similar low contrast lesions being present in MR images. The approaches for detecting MS lesions [21], [22] use texture features and take advantage of the knowledge that MS occurs in a specific tissue type, which is consistently located in similar anatomical regions. This is a type of context (anatomical context) that can be exploited easily for MS, but mTBI lesions do not have this advantage since mTBI can occur in different tissue types.

Recently, Tu and Bai [19] proposed autocontext is a way to model context at the voxel level. The main premise is to estimate an object with a discriminative classifier and use a sampling of the estimated posterior probability as an additional feature to a subsequent classifier. It is able to take information from far away (across the brain) compared to other methods like CRFs [18] which are local. The context features in this case are a sparse sampling of a distant neighborhood around every pixel. This can lead to overfitting due to the very specific locations and this can be seen in one of the examples in [19]. Other methods that exploit this type of context include [23], which has similar pitfalls as autocontext. These methods have been shown to segment rigidly positioned objects well, such as organs or body parts. In this paper, we adopted the idea of cascading classifiers, but developed features that are more generalizable and integrate temporal information, which has not been addressed in [19].

B. Contributions

The contributions of our paper are 1) development of three new contextual features to be used with a cascade of classifiers. These features include a proximity feature, a directional feature, and a maximum *a posteriori* edge distance feature. 2) Use of a temporal sequence of MR images to provide context from a previous time point, capturing the dynamics of the injury progression automatically. 3) Analysis of multiple contextual feature configurations on a rat controlled cortical impact (CCI) mTBI model dataset. This work extends the conference proceedings [37].

III. TECHNICAL APPROACH

A. System Overview

A discriminative approach is taken, where classifiers are used to directly estimate the posterior probability of lesion and normal appearing brain matter (NABM) voxels (note the groundtruth is obtained from segmentation of the mTBI lesion by a domain expert). The discriminative approach performs well when there is a large amount of training data and it can be used for a complex decision space. A voxel level classifier has a large amount of data considering the 3-D nature of MR images. The appearance of lesions in MRIs can be very complex, which leads to a complex decision space.

A cascade of classifiers is used for estimating the detected lesion at each time point (shown in Fig. 2), where information from a previous time point is propagated forward. The first classifier in the cascade estimates the lesion using only the visual features. Then, context features are formed from the posterior probability map estimated by the classifier. These features are recalculated for each iteration in the process, for a given number of classifiers shown as a column of classifier for a single time point in Fig. 2. Spatial information is propagated by the contextual features leading to improved classification. This process was introduced by [19] for static images. The contextual features used by [19] were point samplings of the posterior estimates. Their features demonstrated good segmentation performance on objects that were rigid in shape, when that shape was distorted their performance faltered. We propose two new features that generalize the static contextual information so it will work with amorphous objects.
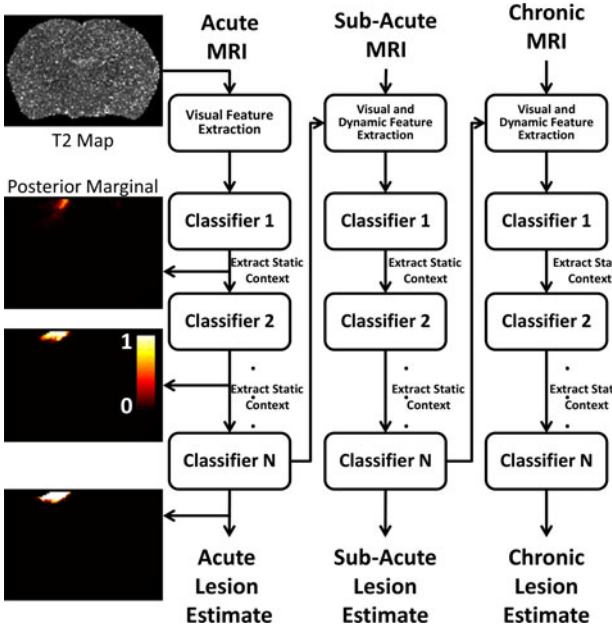
Fig. 2.   Overview of the proposed system. Context information is sent from one classifier to the next. After each classifier the static contextual features are extracted. The output of the *N*th classifier is the final estimate of the lesion for the given time point. The dynamic contextual features are estimated from the final posterior marginal of the preceding time point.

Dynamic contextual features are calculated from the final classifier at a single time point. These features also in our approach are used by the classifier at the subsequent time point, and they make use of spatial and lesion growth information. Note that [19] proposed using spatiotemporal volumes with their basic point features in the higher dimensional space. Their approach would require extreme amounts of data and the entire sequence to be known before segmentation. Our approach only considers pairs of brain volumes at a time, which allows for estimation at every time point.

B. Visual Features

Due to the low contrast nature of the unimodal MR images and the mild nature of the TBI, texture features are used to increase the discrimination in our approach. Four types of texture features are used: uniform local binary pattern (ULBP) local histograms [24] in the coronal plane (59 features), local statistics (mean, variance, skewness, kurtosis) of a Gabor filter bank [25] with eight orientations and four scales in the coronal plane (128 features), basic histogram of oriented gradients in the coronal plane [26] (nine features), and local neighborhood statistical features (mean, variance, skewness, kurtosis, range, entropy, gradient magnitude xyz) (nine features). This gives a total of 205 visual features. This wide variety of features provides many different characteristics without being too specific (i.e., they will generalize well). The size of the local neighborhood used is 5×5 voxels [33], where the feature size is chosen to be the one that maximizes the Bhattacharyya distance between the two classes and gives a bound on the Bayesian error [27]. Examples of the visual features are shown in Fig. 3.

C. Static Contextual Features

The contextual features come from the posterior probability estimated by an already learned classifier. Previous approaches [13] have directly sampled a dense neighborhood around an observed voxel, making each location a potential feature. This method can lead to large feature sizes and can cause overfitting due to the specific locations that are learned. In this paper, two new static features are proposed to overcome this problem. One incorporates a sense of the surrounding without a known direction, while the other gives a general sense of direction.

The first feature, shown in Fig. 4(a), gives the average posterior probability at various distances around the observed voxel. This can be thought of as a proximity feature, where what is a close, medium, and far away in distance are estimated. The distance function used here is the Manhattan distance allowing for a cuboidal region. These features are directionally invariant and can lead to better generalization since they describe a general area. By having a nesting of boxes the integral image can be utilized for quick computation of the features. In 3-D, only eight points are needed to find the average of a cuboidal region, using integral images [28]. Equation (1) provides these features, where f_{xyz} is the proximity feature, R_{1xyz}, R_{2xyz} are square neighborhoods around the voxel at *xyz*, and size(*) is the size of the bounding box

$$f_{xyz} = \left(\sum R_{1xyz} - \sum R_{2xyz} \right)$$
$$\times \left(\frac{1}{\mathrm{size}(R_{1xyz}) - \mathrm{size}(R_{2xyz})} \right). \qquad (1)$$

Directional information is important for classification since the objects are rigidly registered to a naïve animal. The second contextual feature describes the posterior probability in various directions from the observed voxel. Rays are sampled at various distance ranges and angles from the observed voxel [see Fig. 4(b)]. From the distance ranges along the rays the mean is calculated. This gives a refined sense of the surrounding. An example would be what is close and above the observed voxel. The integral image is also used to calculate these features. Both features can be computed at coarse or fine distance bins without a significant increase in computational time. Equation (1) can also be used for the direction context features, the shape of the features are changed to be that of Fig. 4(b). The features are rectangles with width one and the 45° features can be estimated using the rotated image.

D. Dynamic Contextual Feature

We propose the posterior marginal edge distance (PMED) feature as a measure of the distance a voxel is from the perimeter of objects of a class found by the maximum posterior marginal (MPM) estimate. To create this feature, first the MPM at a voxel is obtained from the output of a classifier. This gives a binary image for each class. The distance transform is applied to the
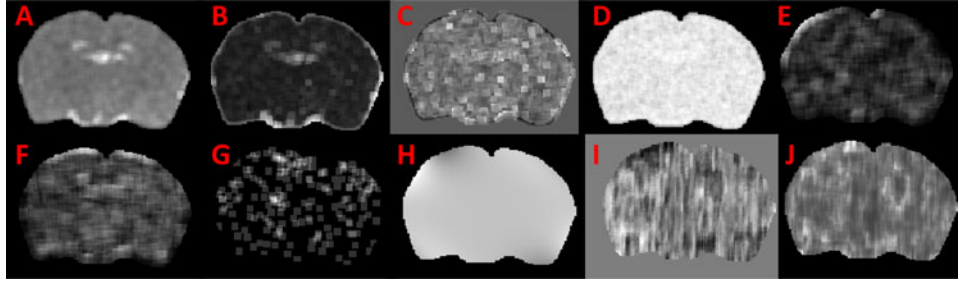
Fig. 3. Examples of the visual features on coronal slices. The features from left to right, top to bottom: (A) local mean, (B) variance, (C) skewness, (D) kurtosis, (E–F) a bin from the histogram of oriented gradients, (G) a bin from the LBP histogram, and (H–J) example gabor features.
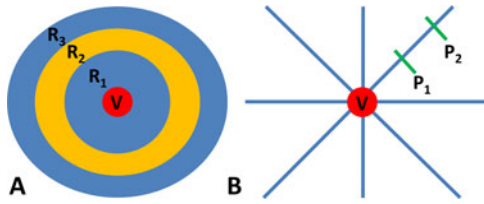

Fig. 4. (A) Illustration of the proximity feature. V is the observed voxel and the feature is the average probability of the regions (R_1, R_2, R_3). (B) Illustration of the distance features. V is the observed voxel and an example feature is the average probability between P_1 and P_2 along the 45° ray.
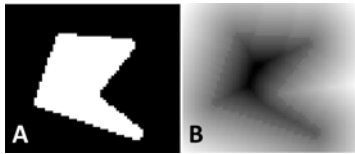

Fig. 5. (A) Example MPM estimate. (B) Corresponding PMED feature. Note that the values become more negative toward the center of the object and more positive farther away from the object.

image and the inverse image and the feature are given by

$$\text{PMED} = d\,(\text{MPM}) - d(\sim\text{MPM}) \quad (2)$$

$$\text{MPM} = \underset{c}{\arg\max} \, p\,(\omega = c|F). \quad (3)$$

Where, $d(*)$ is the Euclidean distance transform. This gives an image that is increasing as the voxels become farther away from the edge and smaller (more negative) as the voxels get further into the object. In (3), ω is the estimated class, c is a specific class (lesion or normal brain in our case), and F is the feature set at a given voxel (see Fig. 5).

E. Classifier Cascade Selection

The base classifier in the cascade of classifiers has to be able to deal with a large number of features, a complex decision space, and be able to give a posterior estimate. The primary classifier being used is adaboost [29] with small decision trees as base classifiers. Using small trees as a weak classifier ($h(*)$) allows for inherent feature selection, meaning erroneous features are disregarded. It is also not sensitive to feature normalization. In each iteration (t), the best classifier is selected and weighted with

ALGORITHM I
ADABOOST

1:	Input(x,y) where x is the set of all training features and features and $\mathbf{y}$ is the class label.
2:	T = number of weak classifiers
3:	Initialize $\boldsymbol{D}_1 = 1/m$ where $\boldsymbol{D}$ is the weight of each training example and m is the number of training examples.
4:	For $t = 1$ to T
5:	$h_t = \arg\max_{h_t \in H} |0.5 - \varepsilon_t|$ // Base Classifier where $\varepsilon_t = \sum D * \sum Cost\,Matrix * (y \neq h_t(x))$ //Error
6:	$\alpha_t = \frac{1}{2} \ln\left(\frac{1-\varepsilon_t}{\varepsilon_t}\right)$ // Classifier Weight
7:	$\boldsymbol{D}_{t+1} = \frac{\boldsymbol{D}_t * \exp(-\alpha_t \mathbf{y} h_t(\mathbf{x}))}{\mathbf{Z}}$ // Reweight the examples Where $\mathbf{Z}$ is a normalization term.
8:	Exit if $|0.5 - \varepsilon_t| < \text{threshold}$ //exit if error is small

α. During the training process a *cost matrix* (4) is used, where the top row represents the cost of normal appearing brain matter (NABM) and the bottom row the cost of Lesion voxels, such that the priors are offset to be even. This is done to account for the large disparity, in the number of training samples between the classes. Algorithm 1 describes the flow of adaboost

$$\text{Cost Matrix} = \begin{bmatrix} 0 & 1 \\ \dfrac{\sum \text{NABM voxels}}{\sum \text{Lesion voxels}} & 0 \end{bmatrix}. \quad (4)$$

It has been shown that the posterior marginal can be estimated using logistic regression [30] given by

$$p(\omega_{xyz} = c|f_{xyz}) = \frac{e^{H_c(f_{xyz})}}{\sum_{c=1}^{C} e^{H_c(f_{xyz})}} \quad (5)$$

$$H_c(f_{xyz}) = \sum_{t=1}^{T} \alpha_t h_t(f_{xyz}). \quad (6)$$

Other classifiers such as the popular support vector machine (SVM) approach are also able to estimate the posterior marginal [31]. SVM is a strong classifier, but it does not have inherent feature selection and is sensitive to feature normalization. SVM tends to perform well with a small number of strong features. An example of the iterative training process for a single time point is shown in Fig. 6. Notice that the estimate improves the greatest between classifier 1 [see Fig. 6(b)] and classifier 2 [see Fig. 6(c)]. During training, each successive classifier will have a performance greater than or equal to its predecessor, since the posterior marginal is one of the features.
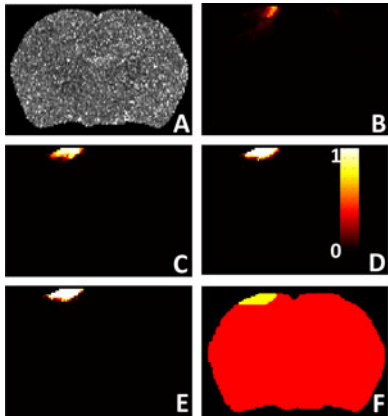
Fig. 6. Example probability maps after each classifier. (a) T2 map. (b–e) Classifier output probability map for the training of classifiers 1–4, respectively. (f) Manual Segmentation where yellow denotes the lesion. This shows the convergence of the algorithm to the manually segmented injury.
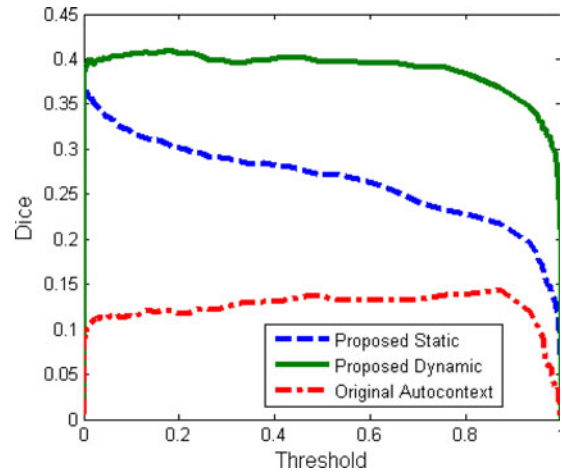

Fig. 7. Dice coefficient after thresholding the posterior probability map at the end of each cascade of classifier (i.e., at each time point). This is the average of all the tests in the leave one out validation.

IV. EXPERIMENTAL RESULTS

A. Contribution of Features in a Temporal mTBI Dataset

Our temporal dataset uses Sprague Dawley rats subjected to a single impact CCI as an animal model of mTBI [13], [32]. The CCI model results in a focal injury. Briefly, a craniectomy (5 mm) was performed over the right hemisphere (3 mm lateral, 3 mm posterior to bregma), where a mild CCI was induced using an electromagnetically driven piston (4 mm diameter, 0.5 mm depth, 6.0 m/s). The incision made for the craniectomy is sutured after the injury is induced.

The animals were imaged *in vivo* at three time points post injury: acute (1st day), subacute (8th day), and chronic (14th day). There are a total of six sequences, each with three time points. MRI data were acquired using a Bruker Advance 4.7T for T2 weighted images (T2WI; $\mathrm{TR/TE/FA} = 3453$ ms/20 ms/20°, 25×1 mm slices) with a 256×256 matrix and 3 cm field of view. Each voxel has a dimension of $0.12 \times 0.12 \times 1$ mm. The T2 weighted images were converted to T2 maps. ROIs were manually segmented using Cheshire image processing software (Hayden Image/Processing Group, Waltham, MA, USA) and included the right and left hemispheres and injured tissue volumes that were defined as abnormal (hyper/hypointense) signal intensities within the cortex with the remaining tissues designated as NABM. The injuries have been verified with histology in [32] at the end points of experiments. A direct comparison to the results of histology is not possible due to the deformations that occur in the histological staining process.

We examine the effect of the proposed features and effect of the dynamic information. For the training/testing split, leave-one-out validation is used where a whole sequence is left out (resulting in six crossfolds). Three temporally consecutive volumes were left for testing and the rest were used for training. The parameters used were: 300 weak learners, learning rate 1, and 4 cascaded classifiers. Three approaches were tested: the original autocontext features [19], the proposed approach with only the proposed static features, and the proposed approach with the static and dynamic features.

To evaluate the segmentation results of the proposed approach the dice coefficient is used, given by

$$\mathrm{Dice} = \frac{2\mathrm{TP}}{(\mathrm{TP} + \mathrm{FP}) + (\mathrm{TP} + \mathrm{FN})} \qquad (7)$$

where TP is true positive, FP is false positive, and FN is false negative. The dice coefficient gives the ratio of the intersection between the detected object and the target object to the size of the objects. The dice gives a better idea of the intersection between the two objects because it does not consider the true negatives, which will be large with the unbalanced class size. The output of the classifier at each time point (acute, subacute, and chronic) shown in Fig. 2 is thresholded to get a hard classification.

From Fig. 7, it is clear that the proposed dynamic approach outperforms the other methods. This shows it is important to use the dynamic information. The original autocontext tends to overfit due to the specific locations the features represent. The same features locations proposed in [19] were used for the original autocontext testing. During the training phase it obtains a dice score above 0.9, but it does not generalize well to the testing data. From the testing, our proposed static features give a good generalization compared to the original autocontext. The output from the original autocontext approach is patchy with many false negatives leading to an underestimation of the injury. This is due to the fact that it looks at specific locations for the context features.

The proposed approach has a very flat dice curve, so it is not sensitive to a chosen threshold on the output probability map. This makes the selection of a threshold less critical. From the qualitative results (see Fig. 8), it is clear that the results of proposed approach work on small to medium size lesions. The qualitative results also show that false positives are only close to the majority of the lesion mass without having erroneous spatial outliers. It is also apparent that the approach has some difficulties at the edges of the lesions. This could be rectified by using shape constraints on the thresholded probability map.
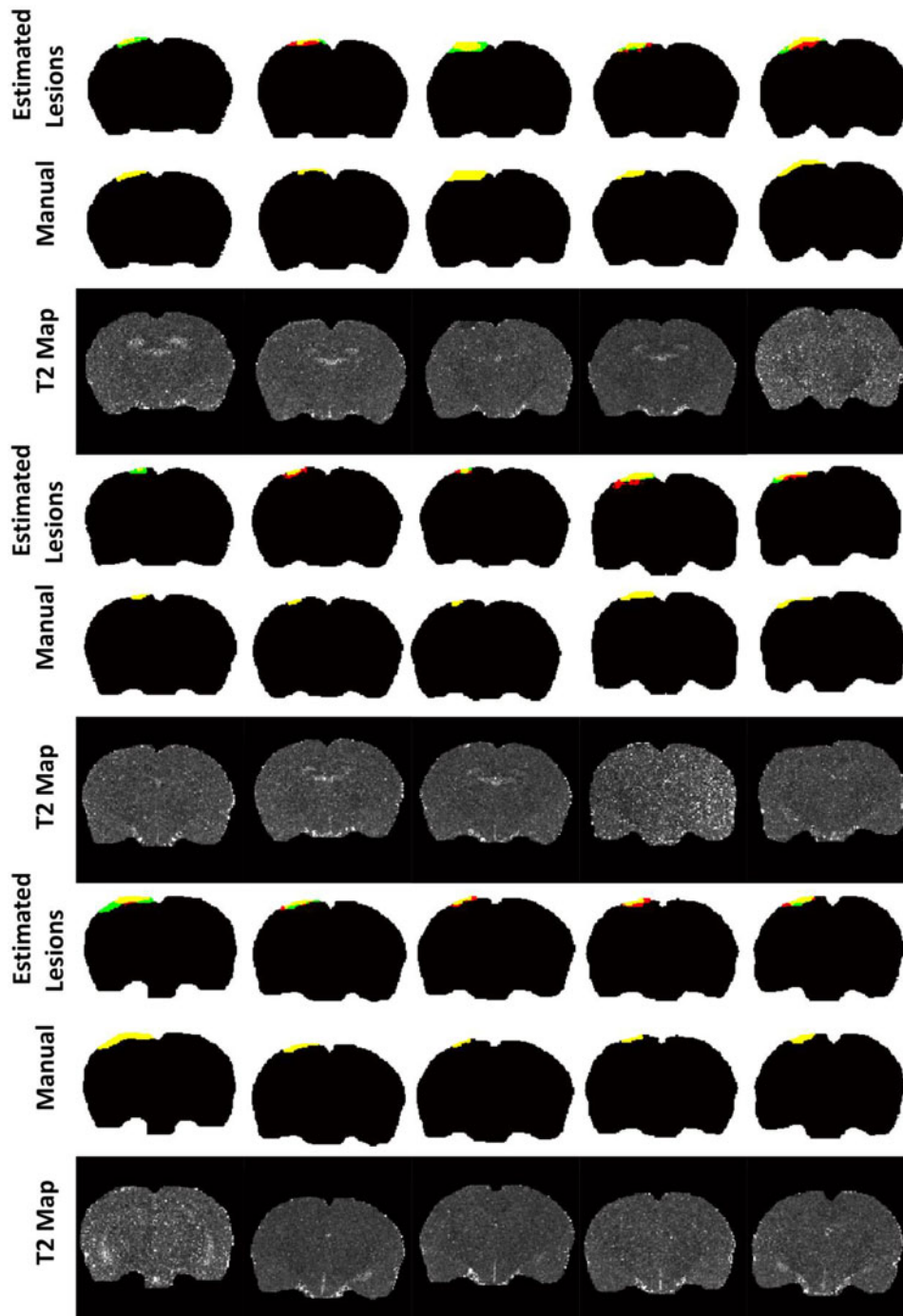
Fig. 8.   Qualitative results of the proposed approach using dynamic and static contextual features. Each coronal slice is from a separate volume. *Color code:* yellow = true positive, black = true negative, green = false negative, red = false positive.

In [20], a similar dataset was used for analysis except repeated contralateral injuries were also considered. The average dice score using a high-level contextual model was 0.35 and 0.07 using probabilistic SVM alone. This is similar to our dice score using the proposed static features with an average dice score of 0.36 and it far exceeds the results of a probabilistic SVM. The dynamic features increase the dice up to 0.41. The method proposed here does not use any extra patient information as it has been done in [20].

B. Convergence Rate of the Features

We evaluate the strength of the individual features. The same dataset from Section IV-A is used in this section. To determine the strength of the features, the rate of convergence of the cost function during training is observed.

In Fig. 9, the training cost after each tree during the training of adaboost is given. Both the autocontext and the proposed static features have the same results from the initial classifier utilizing
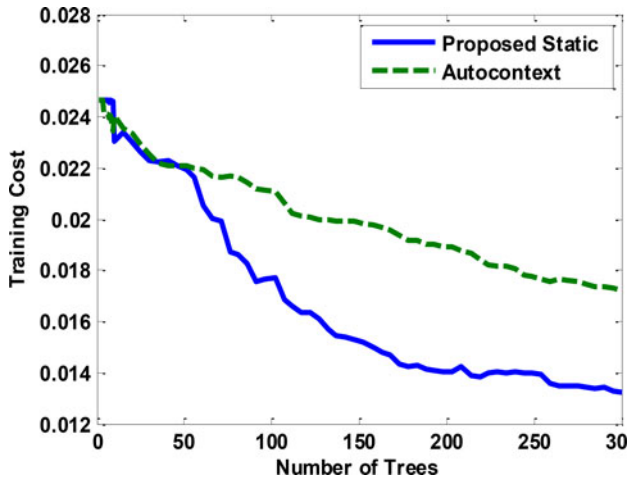
Fig. 9. Training cost after each tree for the proposed static features versus the original autocontext. This is the training cost of the second classifier, i.e., the input to both methods is the results after using visual features only. Lower cost is better.

only visual features. This is due to the proposed static features being able to generalize in the surrounding area better.

To understand the convergence of each classifier in the cascade, one must observe the output training cost after adding each tree during the training of adaboost. In Fig. 10, the convergence of the training using only the static features is observed. Convergence using only the visual features takes a while compared to the static contextual features. After the second classifier, the improvement over the number of trees is less pronounced. Not much information is gained after the second classifier.

Also in Fig. 10, we can observe the convergence of the classifier using the dynamic and static context features. It is apparent that the convergence is very fast for Classifier 1 when the dynamic context features are used, compared to the case when no dynamic information is used in the first iteration. Information is still gained by the static features but at a slower rate.

C. Feature Importance Evaluation

An important question to ask when using adaboost is, "which features are being chosen and when?" Here, those questions are answered by looking at the percent of features chosen throughout the adaboost training process. In the case of the static features alone, Fig. 11 shows first 50 trees are almost exclusively context features. This shows that the contextual features hold the most information for discrimination. The visual features start being used after the information from the contextual features is nearly all used. In the end, 40–50% of all the features are contextual.

A similar pattern occurs when the dynamic features are used (shown in Fig. 11). The contextual features in Classifier 1 are used early in the learning process, and then the visual features almost exclusively take over. In Classifier 3, nearly 60% of the features are chosen as contextual features. This shows that the dynamic information plays a vital role in the classification.

D. Static Feature Performance on the BRATS Dataset

To show the versatility of the proposed approach the static features were tested on a brain tumor dataset. The dataset is
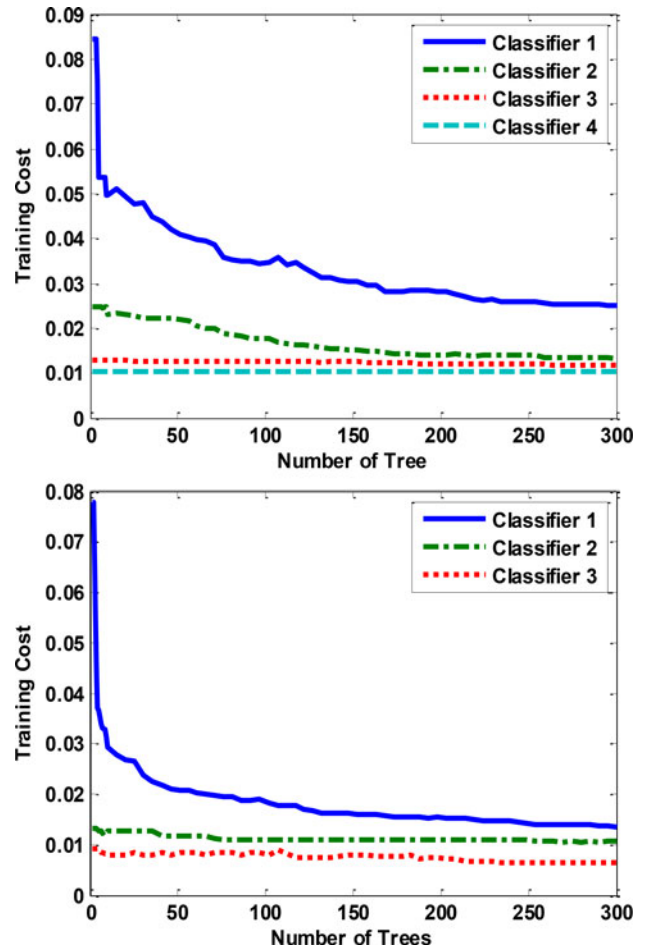

Fig. 10. *Top:* Convergence of classifier training using only the static contextual features. *Bottom:* Convergence of classifier training using both dynamic and static contextual features. Lower cost is better.

from the MICCAI 2012 Multimodal brain tumor segmentation (BraTS) challenge. Here, a subset of the data was used that included 15 High grade glioma patients. The volumes included the following MR modalities, T1, post-Gadolinium T1, T2, and FLAIR. Each modality has been coregistered, skull-stripped, and resampled to be 1 mm isometric voxels. A mode shift was used to normalize the histogram across subjects. For this testing, the edema and core tumor are considered to be a single class. The visual features used were the individual modalities, the same local neighborhood statistics as the mTBI dataset on the FLAIR channel, and LBP on the FLAIR channel. Since there is a single time point database, only the static contextual features are used. Testing was done using 5 fold-cross validation.

For this testing, an average dice score of 0.71 was obtained. The best scores reported during the BraTS challenge were between 0.7–0.8, for the high grade glioma cases. Note that the other approaches [33], [34] used symmetry features. These features can be directly used by the proposed approach. This is another type of context that can be exploited. Another feature used in the challenge were long-range context features [35]. These features sample the value around an observed voxel. The parameter space for these features is extremely large and
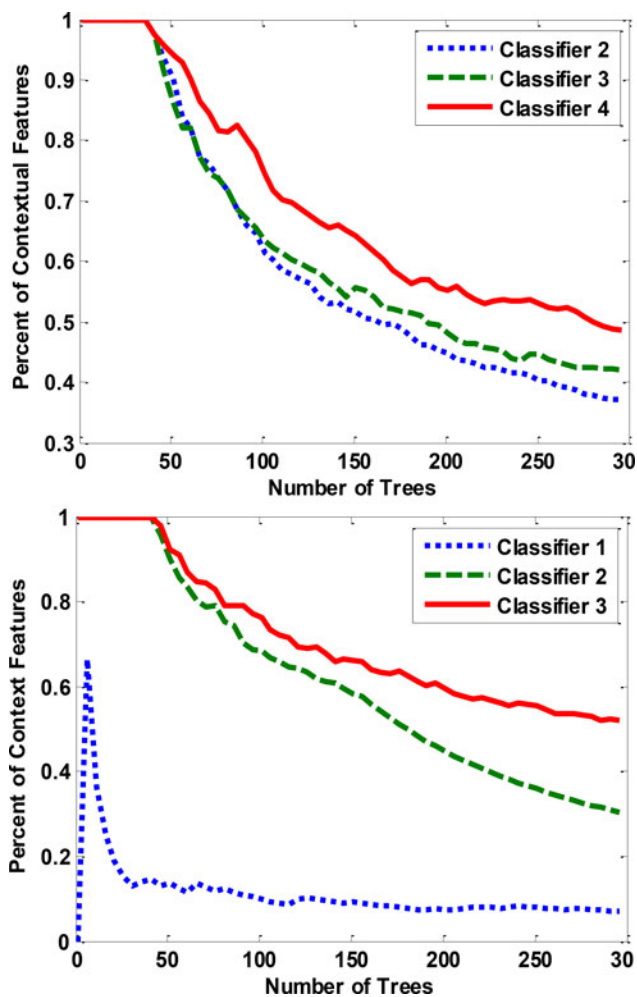
Fig. 11. *Top:* The percentage of the static contextual features chosen versus the current number of trees. *Bottom:* The percentage of dynamic and static contextual features chosen up to a number of trees. Note in Classifier 1 only the dynamic contextual features are used.

requires random sampling of the space via decision forests [36]. The other features used by the winners of the challenge [35] were based on generative modeling of the tissue types. These features can also directly be used by the approach proposed here.

V. CONCLUSIONS

A fully automated method for detecting mTBI lesions that integrates low-level static and dynamic contexts is proposed. Three novel features are proposed that describe the posterior probability of classifier outputs in a cascade. These features were shown to have good qualitative and quantitative results on an mTBI dataset. The proposed approach outperformed the original autocontext [19], by being able to generalize and integrate dynamic information. The context features were shown to be the most important features in the training process. Adding the dynamic context features lead to fast convergence during training leading to a smaller number of trees that are needed. The generality and flexibility of the proposed approach allows it to be applied to other brain lesion problems.

REFERENCES

[1] T. Morris, "Traumatic brain injury," in *Handbook of Medical Neuropsychology*, C. L. Armstrong and L. Morrow, Eds. New York, NY, USA: Springer, 2010, ch. 2, pp. 17–32.

[2] N. C. Colgan, M. M. Cronin, O. L. Gobbo, S. M. O'Mara, W. T. O'Connor, and M. D. Gilchrist, "Quantitative MRI analysis of brain volume changes due to controlled cortical impact," *Neurotrauma*, vol. 27, no. 7, pp. 1265–1274, Jul. 2010.

[3] A. Obenaus, M. Robbins, G. Blanco, N. R. Galloway, E. Snissarenko, E. Gillard, S. Lee, and M. Currás-Collazo. "Multi-modal magnetic resonance imaging alterations in two rat models of mild neurotrauma," *Neurotrauma*, vol. 24, no. 7, pp. 1147–1160, Jul. 2007.

[4] Z. Metting, L. A. Rodiger, J. De Keyser, and J. Van Der Naalt, "Structural and functional neuroimaging in mild-to-moderate head injury," *Lancet Neurol.*, vol. 6, no. 8, pp. 699–710, Aug. 2007.

[5] G. P. Mazzara, R. P. Velthuizen, J. L. Pearlman, H. M. Greenberg, and H. Wagner, "Brain tumor target volume determination for radiation treatment planning through automated MRI segmentation," *Int. J. Radiation Oncol. Biol. Phys.*, vol. 59, no. 1, pp. 300–312, May 2004.

[6] A. Irimia, M. C. Chambers, J. R. Alger, M. Filippou, M. W. Prastawa, B. Wang, D. A. Hovda, G. Gerig, A. W. Toga, R. Kikinis, P. M. Vespa, and J. D. Van Horn, "Comparison of acute and chronic traumatic brain injury using semi-automatic multimodal segmentation of MR volumes," *J. Neurotrauma*, vol. 28, no. 11, pp. 2287–2306, Nov. 2011.

[7] K. Holli, L. Harrison, P. Dastidar, M. Waljas, S. Liimatainen, T. Luukkaala, J. Ohman, S. Soimakallio, and H. Eskola, "Texture analysis of MR images of patients with mild traumatic brain injury," *Biomed. Central Med. Imag.*, vol. 10, no. 8, May 2010.

[8] G. Spitz, J. J. Maller, A. Ng, R. O'Sullivan, N. J. Ferris, and J. L. Ponsford, "Detecting lesions after traumatic brain injury using susceptibility weighted imaging: A comparison with fluid-attenuated inversion recovery and correlation with clinical outcome," *J. Neurtrama*, vol. 20, no. 24, pp. 2038–2050, Dec. 2013.

[9] M. P Quinn, J. S. Gati, L. M. Klassen, A. W. Lin, J. R. Bird, S. E. Leung, and R. S. Menon, "Comparison of multiecho postprocessing schemes for SWI with use of linear and nonlinear mask functions," *Amer. J. Neuroradiol.*, vol. 35, no. 1, pp. 38–44, Jan. 2014.

[10] R. R. Benson, R. Gattu, B. Sewick, Z. Kou, N. Zakariah, J. M. Cavanaugh, and E. M. Haacke, "Detection of hemorrhagic and axonal pathology in mild traumatic brain injury using advanced MRI: Implications for neurorehabilitation," *NeuroRehabilitation*, vol. 31, no. 3, pp. 261–279, 2012.

[11] T. Madhyastha, S. Merillat, S. Hirsiger, L. Bezzola, F. Liem, T. Grabowski, and L. Jancke, " Longitudinal reliability of tract-based spatial statistics in diffusion tensor imaging," *Human Brain Mapp.*, vol. 35, no. 9, pp. 4544–4555, Apr. 2014.

[12] S. N. Niogi and P. Mukherjee, " Diffusion tensor imaging of mild traumatic brain injury," *J. Head Trauma Rehabil.*, vol. 25, no. 4, pp. 241–255, Jul. 2010.

[13] V. Donovan, A. Bianchi, R. Hartman, B. Bhanu, M. J. Carson, and A. Obenaus, "Computational analysis reveals increased blood deposition following repeated mild traumatic brain injury," *NeuroImage: Clin.*, vol. 1, no. 1, pp. 18–28, 2012.

[14] E. D. Bigler and W. L. Maxwell, "Neuropathology of mild traumatic brain injury: Relationship to neuroimaging findings," *Brain Imag. Behav.*, vol. 6, no. 2, pp. 108–136, Jun. 2012.

[15] J. Rajan, D. Poot, J. Juntu, and J. Sijbers, "Noise measurement from magnitude MRI using local estimates of variance and skewness," *Phys. Med. Biol.*, vol. 55, no. 16, pp. N441–N449, Aug. 2010.

[16] A. Bianchi, B. Bhanu, V. Donovan, and A. Obenaus, "Contextual and visual modeling for detection of mild traumatic brain injury in MRI," in *Proc. IEEE Int. Conf. Image Process.*, Orlando, FL, USA, Oct. 2012, pp. 1261–1264.

[17] O. Marques, E. Barenholtz, and V. Charvillat, "Context modeling in computer vision: Techniques, implications, and applications," *Multimedia Tools Appl.*, vol. 51, no. 1, pp. 303–339, Jan. 2011.

[18] J. Lafferty, A. McCallum, and F. Pereira, "Conditional random fields: Probabilistic models for segmenting and labeling sequence data," in *Proc. 10th Int. Conf. Mach. Learning*, 2001, pp. 282–289.

[19] Z. Tu and X. Bai, "Auto-context and its application to high-level vision tasks and 3D brain image segmentation," *IEEE Trans. Pattern Anal. Mach. Intell.*, vol. 32, no. 10, pp. 1744–1757, Oct. 2010.

[20] A. Bianchi, B. Bhanu, and V. Donovan, "Visual and contextual modeling for the detection of repeated mild traumatic brain injury," *IEEE Trans. Med. Imag.*, vol. 33, no. 1, pp. 1–12, Jan. 2014.

[21] P. Anbeek, K. L. Vincken, M. J. P. Van Osch, R. H. C. Bisschops, and J. Van Der Grond, "Automatic segmentation of different-sized white matter lesions by voxel probability estimation," *Med. Image Anal.*, vol. 8, no. 3, pp. 205–215, Sep. 2004.

[22] F. Kruggel, J. S. Paul, and H.-J. Gertz, "Texture-based segmentation of diffuse lesions of the brain's white matter," *NeuroImage*, vol. 39, no. 3, pp. 987–996, Feb. 2008.

[23] A. Montillo, J. Shotton, J. Winn, J. E. Iglesias, D. Metaxas, and A. Criminisi, "Entangled decision forests and their application for semantic segmentation of CT images," *Inf. Process. Med. Imag.*, vol. 6801, pp. 184–196, 2011.

[24] T. Ojala, M. Pietikainen, and T. Maenpaa, "Multiresolution gray-scale and rotation invariant texture classification with local binary patterns," *IEEE Trans. Pattern Anal. Mach. Intell.*, vol. 24, no. 7, pp. 971–987, Aug. 2002.

[25] B. S. Manjunath and W.Y. Ma, "Texture features for browsing and retrieval of image data," *IEEE Trans. Pattern Anal. Mach. Intell.*, vol. 18, no. 8, pp. 837–842, Aug. 1996.

[26] N. Dalal and B. Triggs, "Histograms of oriented gradients for human detection," in *Proc. IEEE Congr. Comput. Vis. Pattern Recog.*, San Diego, CA, USA, Jun. 2005, pp. 886–893.

[27] X. Guorong, C. Peiqi, and W. Minhui, "Bhattacharyya distance feature selection," in *Proc. Int. Conf. Pattern Recog.*, Vienna, Austria, 1996, pp. 195–199.

[28] P. Viola and M. J. Jones, "Rapid object detection using a boosted cascade of simple features," in *Proc. IEEE Congr. Comput. Vis. Pattern Recog.*, Kauai, HI, USA, Dec. 2001, pp. 511–518.

[29] Y. Freund and R. E. Schapire, "A decision-theoretic generalization of on-line learning and an application to boosting," *J. Comput. Syst. Sci.*, vol. 55, pp. 119–139, 1997.

[30] J. Friedman, T. Hastie, and R. Tibshirani, "Additive Logistic Regression: A Statistical View of Boosting," *Ann. Statist.*, vol. 38, no. 2, pp. 337–407, 2000.

[31] J. C. Platt, "Probabilistic outputs for support vector machines and comparison to regularized likelihood methods," in *Advances in Large Margin Classifiers*. Cambridge, MA, USA: MIT Press, 2000, pp. 61–74.

[32] A. Obenaus, M. Robbins, G. Blanco, N. R. Galloway, E. Snissarenko, E. Gillard, S. Lee, and M. Currás-Collazo, "Multi-modal magnetic resonance imaging alterations in two rat models of mild neurotrauma," *J. Neurotrauma*, vol. 24, no. 7, pp. 1147–1160, Jul. 2007.

[33] B. Menze, K. Van Leemput, D. Lashkari, M. Weber, N. Ayache, and P. Golland, "Segmenting glioma in multi-modal images using a generative-discriminative model for brain lesion segmentation," presented at the Med. Image Comput. Comput. Assisted Intervention BraTS Challenge, Nice, France, 2012.

[34] E. Geremia, B. H. Menze, and N. Ayache, "Spatial decision forest for glioma segmentation in multi-channel MRI," presented at the Med. Image Comput. Comput. Assisted Intervention BraTS Challenge, Nice, France, 2012.

[35] D. Zikic, B. Glocker, E. Konukoglu, J. Shotton, A. Criminisi, D. H. Ye, C. Demiralp, O. M. Thomas, T. Das, R. Jena, and S. J. Price, "Context-sensitive classification forests for segmentation of brain tumor tissues," presented at the Med. Image Comput. Comput. Assisted Intervention, Nice, France, 2012.

[36] A. Bianchi, J. V. Miller, E. T. Tan, and A. Montillo, "Brain tumor segmentation with symmetric texture and symmetric intensity-based decision forests," presented at the IEEE Int. Symp. Biomed. Imag., San Francisco, CA, USA, Apr. 2013.

[37] A. Bianchi, B. Bhanu, V. Donovan, and A. Obenaus, "Detecting mild traumatic brain injury using dynamic low level context," presented at the IEEE Int. Conf. Image Process., Melbourne, Australia, Sep. 15–18, 2013.

Anthony Bianchi (S'06) received the B.S. degree in electrical engineering from the California State Polytechnic University, Pomona, CA, USA, in 2008 and the M.S. degree in electrical engineering from the University of California, Riverside, CA, USA, in 2010. He completed his Ph.D. degree in electrical engineering at the Center for Research in Intelligent Systems, University of California, Riverside in September 2014.

He is currently working toward the Ph.D. degree in electrical engineering at the Center for Research in Intelligent Systems, University of California, Riverside.

His research interests include image processing, computer vision, pattern recognition, and machine learning. His current research interests also include mild traumatic brain injury and contextual feature generation.

Bir Bhanu (S'72–M'82–SM'87–F'95) received the S.M. and E.E. degrees in electrical engineering and computer science from the Massachusetts Institute of Technology, Cambridge, MA, USA, the Ph.D. degree in electrical engineering from the University of Southern California, Los Angeles, and the M.B.A. degree from the University of California, Irvine, CA.

He is currently a Distinguished Professor of electrical engineering, a Cooperative Professor of computer science and engineering, mechanical engineering, and bioengineering, and the Director of the Center for Research in Intelligent Systems and the Visualization and Intelligent Systems Laboratory with the University of California, Riverside. In addition, he serves as the Director of National Science Foundation (NSF), The Integrative Graduate Education and Research Traineeship program on Video Bioinformatics and the Interim Chair of the Department of Bioengineering at UCR. He has been the Principal Investigator of various programs for NSF, Defense Advanced Research Project Agency, National Aeronautics and Space Administration, Air Force Office of Scientific Research, Office of Naval Research, Army Research Office, and other agencies and industries in the areas of video networks, video understanding, video bioinformatics, learning and vision, image understanding, pattern recognition, target recognition, biometrics, autonomous navigation, image databases, and machine vision applications. He is the author or coauthor of 450 reviewed technical publications, including more than 125 journal papers and 43 book chapters, seven published books, and three edited books. He is the holder of 18 (five pending) patents. His current research interests include computer vision, pattern recognition and data mining, machine learning, artificial intelligence, image processing, image and video database, graphics and visualization, robotics, human computer interactions, and biological, medical, military and intelligence applications.

Dr. Bhanu is Fellow of American Association for the Advancement of Science, International Association of Pattern Recognition, and The International Society for Optics and Photonics.

Andre Obenaus received the B.S. degree in biophysics from La Sierra University, Riverside, CA, USA, in 1984, and the Ph.D. dgree in neurophysiology from the University of British Columbia, Vancouver, BC, Canada, focused on understanding the mechanisms of epilepsy in 1989. Subsequent postdoctoral fellowship in continued his studies of epilepsy were undertaken at University of California, Los Angeles (UCLA), CA.

In 1995, he received a Research Associate Position in the Department of Neurology at UCLA. From 1996 to 2002, he became an Assistant Professor within the Academic Department of Medical Imaging, the University of Saskatchewan, SK, Canada, where he applied neuroimaging techniques, principally magnetic resonance imaging (MRI) to study epilepsy. These early studies in MRI led to recruitment to Loma Linda University within the Department of Radiation Medicine in 2001, where he was instrumental in establishing the Non-Invasive Imaging Laboratory (NIL). He became the Director of the NIL in 2007 to 2012 overseeing acquisition and management of several MRIs, computed tomography (CT, and positron emission tomography (PET) imagers. His research interests include to identify the biological mechanisms underlying normal and abnormal brain function using imaging modalities. He has 118 peer-reviewed journal articles, including *Journal of Neuroscience* and *Annals of Neurology*. He has also contributed 10 book chapters including methods of computational analysis of MR images.

Dr. Obenaus received several awards including in 1999 a prestigious Medical Research Council Fellowship for 5 consecutive years. He was also nominated to the Faculty of 1000 in 2011 based on work related to tracking and monitoring stem cells within the brain using MRI. In 2012, he became a Member in the Department of Pediatrics, the School of Medicine at LLU.